Original article

Kidney anatomy, histology and histometric traits associated to renosomatic index in *Gymnotus inaequilabiatus* (Gymnotiformes: Gymnotidae)

Carlos Eurico Fernandes, Sandrieley Fernanda Marcondes, Gizela Melina Galindo and Lilian Franco-Belussi

The *Gymnotus inaequilabiatus* is a Neotropical fish widely distributed in marginal areas of bays. The aim of this study was to describe the main histological and histopathological traits in the head and exocrine kidney**.** Here, histometric and structural density techniques were associated with renosomatic index (RSI). The kidney was processed for light microscopy. Lipofuscin and hemosiderin content were visually estimated in the melonomacrophages centers (MMCs). All the biometric body variables were correlated with RSI, especially the kidney weight and gross lesions count. The general architecture of head and exocrine kidney was similar to that described for other teleost species. MMCs were prevalent in both portions and correlated with RSI in the head and exocrine kidney. Granulomatous structures were often observed in both portions; however, they were associated only in the exocrine kidney with RSI. Of all the structures hystometrically estimated, only proximal tubular diameter and thickness, and distal tubular thickness were correlated to renosomatic index. The RSI is an useful biometric variable that represent some physiological and morphological characteristics of kidney in *G. inaequilabiatus*. These findings may be used in future studies to evaluate the effects of environmental stressors on the renal adaptative physiological process.

Keywords: Fish, Pathology, Renal morphology, Stereology, Teleost.

Gymnotus inaequilabiatus é um peixe neotropical amplamente distribuído em áreas marginais de baías. O objetivo deste estudo foi descrever características anatômicas, histológicas e histopatológicas no rim cefálico e exócrino. Análises histométricas e a densidade volumétrica estrutural foram associadas ao índice renossomático (IRS). Fragmentos de ambos tecidos foram processados para análise e microscopia de campo claro. O conteúdo de lipofuscina e hemossiderina foi estimado visualmente nos centros de melanomacrófagos (CMMs). Todas as variáveis corporais biométricas foram correlacionadas com o IRS, principalmente o peso renal e a contagem de lesões superficiais. A arquitetura geral do rim cefálico e exócrino foi semelhante à descrita para outras espécies de teleósteos. Os CMMs foram frequentes em ambas as porções e correlacionaram-se com o IRS. Estruturas granulomatosas foram frequentemente observadas em ambas porções; no entanto, foram associadas ao IRS apenas no rim exócrino. De todas as estruturas estimadas histometricamente, apenas o diâmetro e espessura dos túbulos proximais e distais correlacionaram-se ao IRS. Este índice mostrou-se uma variável útil associada a características fisiológicas e morfológicas do rim de *G. inaequilabiatus*. Esses achados podem ser empregados em futuros estudos a fim de avaliar efeitos ambientais bem como processos adaptativos fisiológicos.

Palavras-chave: Estereologia, Morfologia renal, Patologia, Peixe, Teleósteos

Introduction

The kidney is a representative and integrated organ with many vital functions of the organism. As in other vertebrates, the kidney of fish is the primary organ involved in the osmoregulation process and exerts a critical immunological function (Cuesta *et al.*, 2007; Harper, Wolf, 2009). Anatomically, this organ divides into two portions denominated as cephalic or head, and exocrine or trunk kidney. In some species, no division between portions is observed, although morphology and functions are distinct (Takashima, Hibiya, 1995). The head portion consists of lymphohematopoietic tissue connected by an extensive network of vessels and capillaries drained by the renal portal system (Roberts, 2012). The erythroid, lymphoid, and myeloid cells are situated within a stroma

Laboratório de Patologia Experimental - LAPEx, Instituto de Biociências - INBIO, Universidade Federal de Mato Grosso do Sul – UFMS, Av. Costa e Silva, s/n, Bairro Universitário, 79002-970 Campo Grande, MS, Brazil. (CEF) carlos.fernandes@ufms.br (corresponding author), https://orcid.org/0000-0001-5425-1866, (SFM) sandy.marcondes@outlook.com, https://orcid.org/0000-0002-3439-0022; (GMG) gizelagm73@gmail.com, https://orcid.org/0000-0002-3456-1688; (LFB) lilian.franco@ufms.br, https://orcid.org/0000-0003-1938-8423

of reticuloendothelial tissue in association with mature granulocytes and agranulocytes cells (Zapata *et al*., 1996; Roberts, 2012). The exocrine kidney is comprised of nephrons diffusely distributed, which are still intermediated by hematopoietic and lymphopoietic tissue (Larsen, Perkins Jr., 2005; Menke *et al*., 2011). Although the histological traits of kidney structures are well known in fish the wide variations in their anatomy, histology, and cytology, related to the habitat conditions make this organ play a primordial role in the adaptive and evolutionary processes in fish (Dantzler, 2016). In this regard, few studies have been conducted given the considerable biodiversity of fish species in the Neotropical region, especially from their natural environments.

Organosomatic indices are used to measure organ mass relative to body mass. In association with other body metrics, organosomatic indices have been widely used in ecological and experimental studies (Schlenk *et al*., 2008). However, the renosomatic index has been poorly reported in association with useful histological biomarkers. This index tracks metabolic variations in response to parasite infections, heavy metal contamination, involvement in physiological adjustment to environmental conditions or seasonality (Resende *et al*., 2010; Jordanova *et al*., 2017; Strepparava *et al*., 2018). On the other hand, the quantification of morphometric measurement allows detection of minimal differences in cells and tissues, favoring the qualitative analysis in addition to responding to the functional and pathological changes in an organ (Oberholzer *et al*., 1996; Nyengaard, 1999; Hamilton *et al*., 2014). Therefore, the combined interpretation of this index would permit the assessment of distinct physiological responses from the internal and external individual factors (Dethloff, Schmitt, 2000).

The Gymnotiformes order comprises more than 250 species distributed in 45 *Gymnotus* spp. genera and represent nearly four percent of all ichthyofauna of the Neotropical region (Fricke *et al*., 2019). In the Brazilian Pantanal, *Gymnotus inaequilabiatus* is distributed in marginal areas of bays formed by flooded areas of low and receding waters of rivers that drain into the Paraguay and Parana River, with abundant aquatic vegetation (Resende *et al.*, 2006). The life history and natural habitat of *Gymnotus* spp. suggest that they adapted to low oxygen rates or have a wide capacity for survival in extreme hypoxic environments, probably by an outstanding physiological adaptive process (Crampton, 1998; Moraes *et al*., 2002). On this point, renal histomorphometry assessment can play a key role owing to the functional plasticity of this organ (Sakai, 1985; Resende *et al*., 2010; Hassan *et al*., 2017; Pelster *et al*., 2018).

The Gymnotidae family has been studied from the genetic, taxonomic, endoparasitic fauna and ecological standpoints (Willink *et al*., 2000; Albert *et al*., 2005; Scacchetti *et al*., 2011; Galindo *et al*., 2017). Although these studies are numerous, there are no reports about anatomy, histology, and histopathological features of the kidney and

were not even reported biometrics and histometric traits in this species. Therefore, profiling based on a comparative database following the evolution of histometric traits in specimens under natural habitats might suggest *G. inaequilabiatus* as a potential environmental bioindicator.

This study aimed to characterize and describe the main histological and histopathological finds in the head and exocrine kidney in the *G. inaequilabiatus*. Additionally, histometric and structural density techniques were applied to provide quantitative subsets associating them with the renosomatic index.

Material and Methods

Samples and biometric data. Adult *G. inaequilabiatus* specimens (female, n = 39; male, n = 45) from Porto Morrinho, Corumbá, Brazil, (19°46'49"S 57°41'52"W) were acquired from a fishing community. The specimens were transported in oxygenated polyethylene bags to the laboratory and maintained in aquaria supplied with artificial aeration at constant temperature (25.0°C) until euthanasia (2-Fenoxietanol, 2 mL/L), approximately 3-5 days after transport. Then, the fish were weighed (total weight in grams) and measured (total length in centimeters) to estimate the relative condition factor (Kn) according to the formula $Kn = W/aL^b$, where W is the weight of the individual, L is the standard length of the individual, and *a* and *b* are the constants from the weight-length relation (Le Cren, 1951). After that, the fish were necropsied for kidney analysis. This organ was carefully removed and weighed to calculate the renosomatic index (RSI = kidney weight (g)/body weight (g) x 100). The gross lesions evaluation was conducted on the dorsal and ventral surfaces, considering the number, category, and distribution (Bruno *et al*., 2013).

Histological and histochemical analysis. Fragments of the head and exocrine kidney from 20 specimens randomized (n = 16 females and 14 males) were prepared. After fixation in buffered formalin 10% for 24 hours, the samples were dehydrated in ethanol, embedded in Paraplast Plus (Sigma-Aldrich®) and 5 μm sections were then stained with hematoxylin and eosin (H&E). Masson Trichrome (MT) and Periodic Acid Schiff (PAS) staining were prepared for collagen fibers and glycogen cell deposit analyses (Carson, Hladik, 2009). To detect the lipofuscin content in MMCs, fragments of the same samples were fixed in methacarn solution (60% absolute methanol, 30% chloroform, and 10% glacial acetic). Kidney histological sections were incubated for 1 minute in Schmorl solution, containing 75 mL of 1% ferric chloride, 10 mL of potassium ferricyanide, and 15 mL of distilled water. Next, the sections were immersed in an aqueous 1% neutral red solution followed by 1% eosin. To detect the hemosiderin content, sections were incubated in ferrocyanide acid solution, obtained by dissolving 2 g of potassium ferrocyanide in 100 mL of hydrochloric acid solution 0.75 mmol/L, for 15 minutes, and immersed

in aqueous 1% neutral red followed by aqueous 1% eosin staining (Franco-Belussi *et al.*, 2012). Histological changes, where present, were reported according to morphological characteristics.

Histometry and structural volumetric density analysis. Histometric measures were processed in sections stained by MT. Ten images/section at 400 × magnification, considering at least five structures per image, were used to estimate the renal corpuscle diameter (µm) and area (µm^2), the glomerular area (µm^2), the diameter (µm), and thickness of the proximal and distal tubular epithelium. Additionally, the following parameters were calculated: Bowman´s space area (µm^2; renal corpuscle area – glomerular area), the glomerular area/renal corpuscle area ratio (Rgrc = glomerular area/ renal corpuscle area x 100) and Bowman´s space area/renal corpuscle area ratio (RBrc = Bowman's space area/renal corpuscle area) x 100. The Motic Image Plus 2.0 (Motic Asia) software was used for this analysis.

For the structural volumetric density analysis, images were captured with a Leica DF495 camera coupled to a bright light microscope (Leica DM5500 B). The volume densities were prepared using sections stained by H&E. Digital graticules overlapped ten images at 400 x magnification with 266 intersections. Subsequently, lymphohematopoietic tissue, melonomacrophages centers (MMCs), blood vessels, sinusoidal spaces, and general tissue alterations were estimated in the head kidney. All these structures, in addition to the glomerulus, proximal, and distal tubules, were assessed in the exocrine kidney. Then, the following formula was applied: Dv (%) = (Ps x 100) / Pr, where Ps is the number of intersections counted for each structure, and Pr is the total number of intersections (Freere, Weibel, 1967; Reid, 1980; Rocha *et al.* 1997). The ImageJ 1.45M software was used for this analysis.

Statistical analysis. Data were tested for normality and homogeneity by Kolmogorov-Smirnov test and the Shapiro-Wilk's W test. Blood vessels and granulomatous lesions from the structural density analysis were arcsine transformed. No differences were observed between females and males (P > 0.05, one-way ANOVA, t-test) in the entire population (n = 89) and that randomized to the histological analysis (n = 20). Then, the overall mean, standard deviation, and percentis (25th and 75th) were predicted. Pearson's correlation estimated linear correlations between biometrical, structural volumetric densities, and histometric measures with RSI. SPSS 17.0 (IBM®) software was used in the analysis.

Results

Biometric variables such as body weight, length, kidney weight, relative condition factor (Kn), and RSI for the whole population, are reported in Tab. 1. The RSI was correlated to all biometric variables. The highest correlations were found with kidney weight and gross lesions count.

Tab. 1. Descriptive statistic values for biometric variables, gross lesions. sd, standard deviation; *r*, Pearson's correlation coefficient, * $p < 0.05$; ** $p < 0.01$.

	Percentis			*r*
	Mean (±sd)	25th	75th	
Body weight (g)	125.0 ±43.4	110.7	155.4	0.28**
Total length (cm)	32.9 ±4.31	31.7	35.7	0.21*
Kidney weight (g)	0.70 ±0.32	0.60	0.89	0.63**
Relative condition factor (Kn)	1.92 ±0.20	1.93	2.04	0.27*
Gross lesions (n)	3.2 ±2.1	1.5	5.0	0.48**
Renosomatic index (%)	0.55 ±0.11	0.47	0.64	-

The kidney of *G. inaequilabiatus* is situated in the dorsoventral and retroperitoneal region of the coelomatic cavity. It is composed of two cranial branches or lobes, which comprise the head portion of the kidney. These branches are an extension of the exocrine part of the organ. The color was typically dark brown; however, some samples presented a dark red color. The majority of the lesions were rounded with focal distribution, and whitish displaying regular nodules often raised from the surface. Submacroscopic images revealed the MMCs diffusely distributed in both head and exocrine kidney (Fig. 1).

The histological architecture of head and exocrine kidney is similar to other freshwater teleosts (Fig. 2). The parenchymal arrangement is diffusely distributed without anatomical divisions between glomeruli and excretory structures. Lymphohematopoietic cell niches compose the head organ as a continuity of interstitial tissue observed throughout the exocrine segment. In low magnitude, it was possible to see the transition region between exocrine and head kidney. The sinusoidal networks were widely distributed from the capillaries, vessels, and arterioles (Figs. 2a–b). In addition to undifferentiated hematopoietic cells, macrophages, lymphocytes, granulocytic cells, and rodlet cells were found in both head and exocrine kidney. The collecting tubules (rarely seen) displayed tall and narrow columnar cells with nuclei basally situated. The MMCs, which present several shapes and sizes, were observed in both head and exocrine hematopoietic tissue. As to other freshwater fish, the proximal tubules present columnar cells with brush border; however, distal tubules do not have this characteristic. The cells of both segments showed similar size, although the proximal tubules were slightly more eosinophilic. Nuclei were basally located in proximal and distal tubular segments, and a lesser amount of central and apical location was also observed (Figs. 2c–d). Hyaline degeneration of the tubular epithelium was randomly found, without, however, joining with other degenerative forms. Stannius corpuscle is localized in the middle region of both branches from the head kidney, covered by a capsule of connective tissue that extends into the corpuscular space. The glandular lobules are constituted by numerous granule cells enclosed by sinusoidal capillary plexus (Figs. 2e–f).
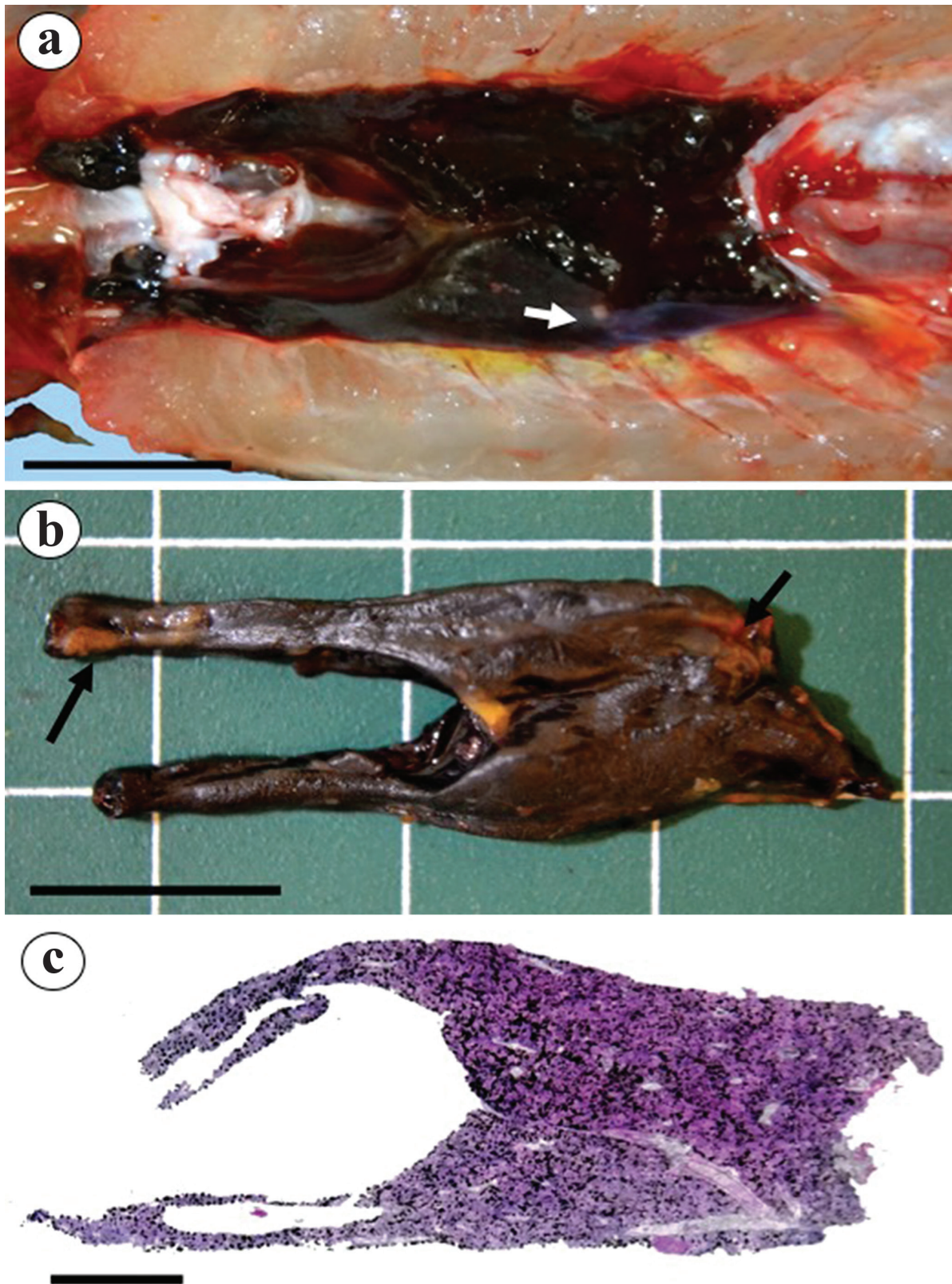
Fig. 1. Macroscopic and submacroscopic aspects of the kidney in *Gymnotus inaequilabiatus*. **a.** anatomical position; dorsal to the ventral vertebral column. The branches of the head portion are narrow and separated by healthy connective tissue (white color). The organ was not fixed and shows the natural color ranging from dark brown to black. Note a rounded and whitish lesion (arrow). **b.** dissected organ post-fixation process. The arterial vessel is positioned on the ventral side (arrows). **c.** submacroscopic aspect showing the MMCs diffusely distributed in both head and exocrine kidney. Bar scale = 1 cm.
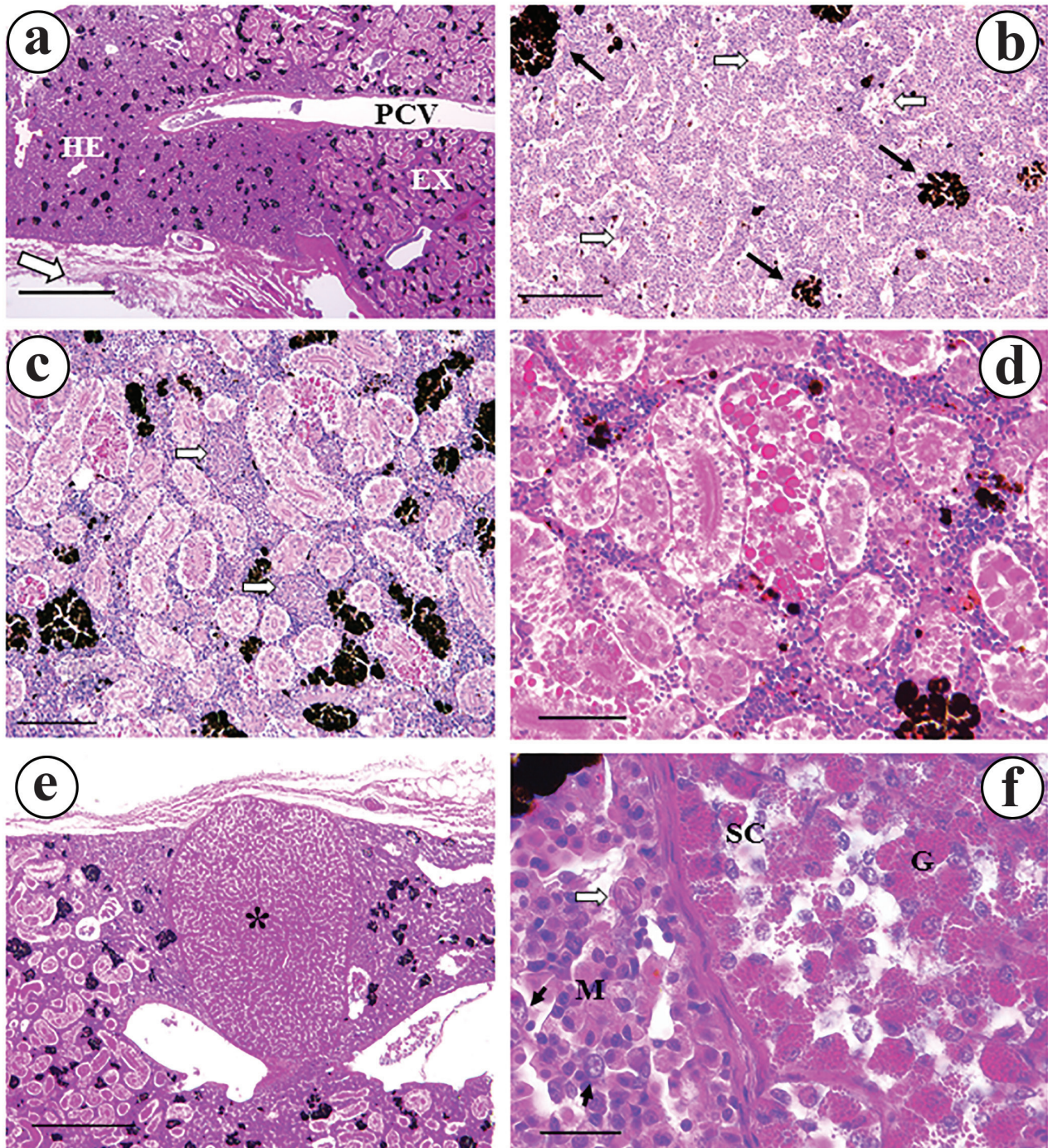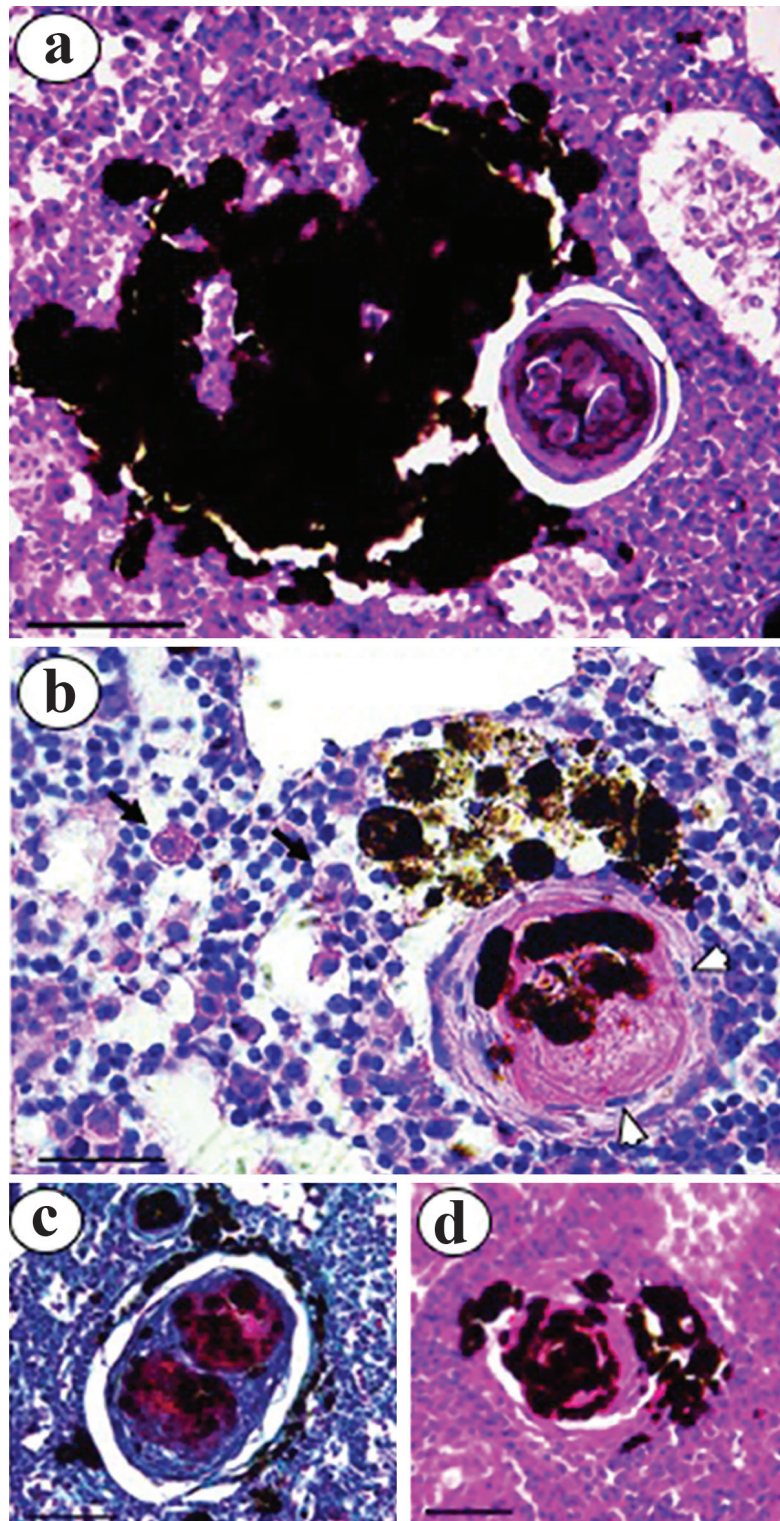
Fig. 2. Cross-section of the head and exocrine kidney in *Gymnotus inaequilabiatus*. **a.** a transitional area between head (HE) and exocrine kidney (EX) drained by postcardinal vein (PCV). Lymphohematopoietic tissue is abundant in the head portion. MMCs are diffusely distributed in both portions. A thick fibrous capsule covers the organ (white arrow); HE, bar scale = 500 µm. **b.** the general aspect of the head kidney. Vascular sinusoids (white arrows) surrounding the lymphohematopoietic tissue enclosing the MMCs (black arrow); HE, bar scale = 200 µm. **c.** interstitial lymphohematopoietic tissue with MMCs deposits characterizes the exocrine kidney, in addition, the contoured tubules; renal corpuscle (white arrow); HE, bar scale = 200 µm. **d.** the exocrine kidney with a proximal convoluted tubule showing hyaline degeneration of the tubular epithelium often found in this species; HE, bar scale = 100 µm. **e.** exocrine kidney showing the corpuscle of Stannius (*). This structure is not lobulated, and is delimited by a fibrous capsule, and situated at the junction between head and exocrine portions; HE, bar scale = 500 µm. **f.** detail of junction between lymphohematopoietic tissue and corpuscle of Stannius in the head kidney. Fiber bundles subdivide both structures. Rodlet cells (white arrow), macrophages (M) and eosinophilic granulocytic cells (black arrow); granulocytic (G) and secretory cells (SC) internally fill the corpuscle; HE, bar scale = 50 µm.

Renal corpuscle (glomerulus and Bowman´s capsule) is filled by a parietal epithelium closed to the interstitial cells, proximal and distal tubules. Visceral layer (podocytes), mesangial cells, capillary, and intracapsular space were identified in the glomerulus. Collagenous structures permeate the intracapsular space and outline of all structures (Figs. 3a–b). The lipofuscin and hemosiderin histochemical reactions in the MMCs are displayed in Figs. 3c–f. Hemosiderin and lipofuscin were observed more in the exocrine kidney in contrast to the head. Granulomatous structures were often observed in both kidneys. Usually, the MMCs were found surrounding or inside the granulomas. Internally, the granulomas were typically constituted of cell debris, necrotic material, and collagen fibers. Rodlet cells were observed peripherally to MMC aggregates associated with lymphocytes, macrophages, and eosin granulocytic cells (Fig. 4).
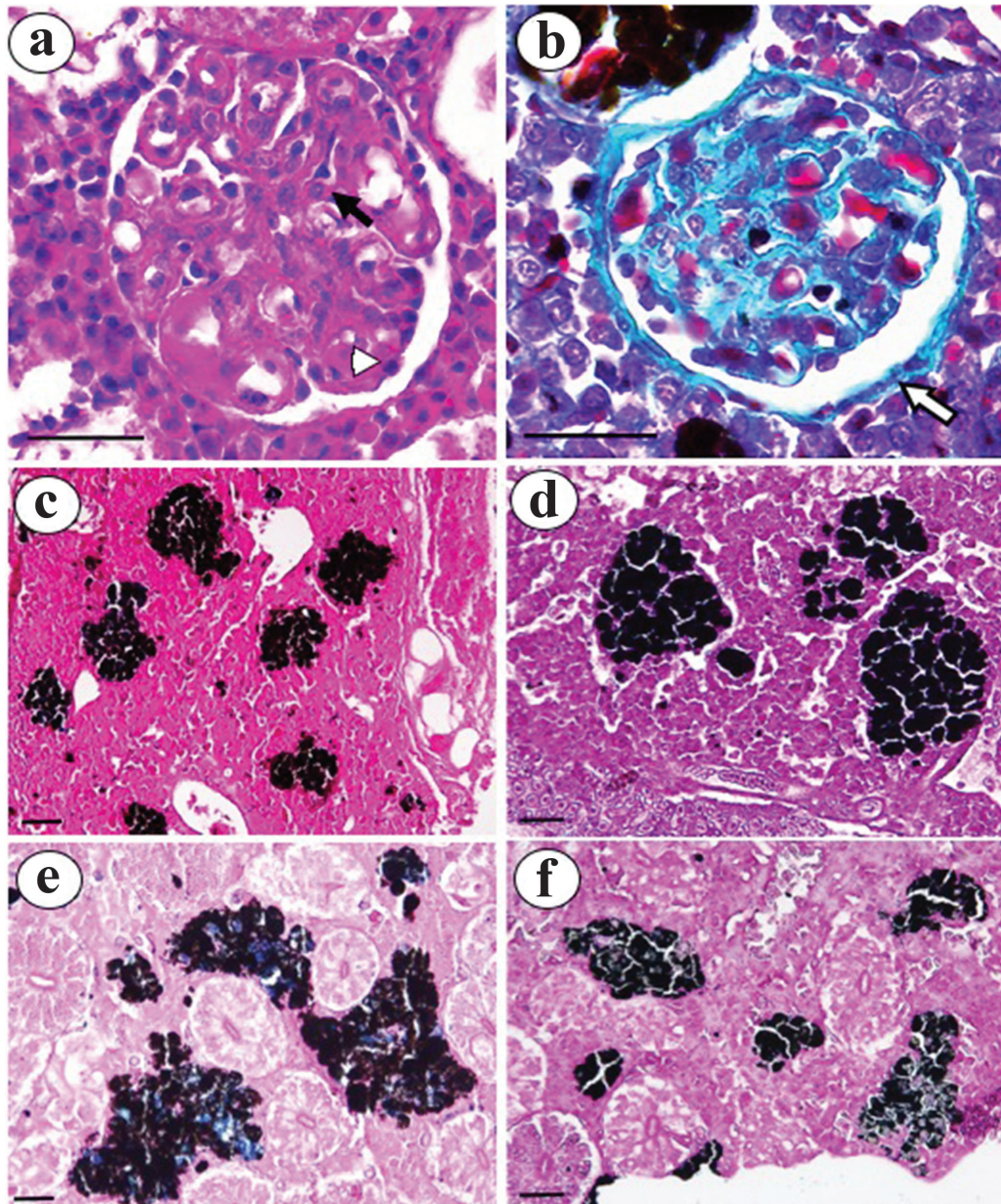
Fig. 3. Histological cross-sections and histochemical reactions to hemosiderin and lipofuscin in the kidney tissue of *Gymnotus inaequilabiatus*. **a.** typical architecture of renal corpuscle with central vascularized area characterized by a clump of capillaries closed to mesangial cells (black arrow) and podocytes (white arrowhead) surrounded by Bowman's capsule; HE, bar scale = 10 μm. **b.** the glomerular capsule encloses the outer fibrous layer (white arrow) and filled by connective tissue. Red cells are inside capillaries; TM, bar scale = 10 μm. **c–f.** MMCs stained with ferrocyanide acid solution to hemosiderin and Schmorl´s solution to lipofuscin. **c.** melanin predominance in the head kidney MMCs. **d.** slight labeling to lipofuscin in the head kidney MMCs. **e.** positive labeling to hemosiderin (blue color) conjoined to the melanin deposits in the exocrine kidney. **f.** positive staining to lipofuscin (grayish blue color) in the exocrine kidney; Bar scale = 25 μm.

Fig. 4. Histological cross-sections of the head and exocrine kidney demonstrating different granulomatous structures in *Gymnotus inaequilabiatus*. **a.** severe aggregation of MMCs outer to granuloma in the exocrine kidney; PAS, bar scale = 20 µm. **b.** a clump of melanogenic macrophages (dark pigmented cells) adjacent to granuloma in the head kidney. The hematopoietic tissue is edematous and atypical. Some rodlet cells (black arrow) are observed. Granuloma presents a compact and thick layer of collagen with internal necrotic content surrounded by epithelioid cells (white arrows); H&E, bar scale = 10 µm. **c.** two well-defined granulomas with substantial internal necrotic content involved by fibrous tissue. A slight layer of MMCs aggregates close to the external wall of granuloma. TM, bar scale = 10 µm. **d.** MMCs aggregates both internally and externally to granuloma in the exocrine kidney. HE, bar scale = 10 µm.

The lymphohematopoietic tissue was the most critical structure of the head and exocrine kidney (Tab. 2). In the head portion, it was followed by the sinusoid lumen and MMCs. Blood vessels and granulomatous lesions were poorly observed; however, both showed a higher variation (standard deviation superior to mean). Low linear correlation coefficients for lymphohematopoietic tissue and MMC volumetric density were estimated. In the exocrine kidney, the percentage of proximal tubules was close to hematopoietic tissue. Distal tubules and MMCs were equivalents, and granulomatous lesions were higher in the head kidney. The glomerulus was the least dense structure, representing approximately 0.41–0.63% of all exocrine kidney parenchyma. Granulomatous lesions were more prevalent in the exocrine kidney. Except for renal corpuscle, all the structures correlated to RSI.

The histometric measures dataset is reported in Tab. 3. The glomerular area represented approximately 83.9 % of the renal corpuscle while the Bowman´s space approximately 16.0 %, although a high range has been observed. The proximal tubular diameter and thickness of the epithelium were larger concerning distal tubular measures. Of the all structures measured, only proximal tubular diameter and thickness, and distal tubular thickness were correlated to RSI.

Discussion

The selective habitat and wide-ranging distribution in the Neotropical region make the *Gymnotus inaequilabiatus* a notable species to explore physiological and adaptive responses concerning its environment and life history. Typically, this species remains in lotic environments submerged in the mud closest to macrophyte vegetation. These conditions are characterized by low oxygen level, which probably induces anatomical and functional adaptations, such as breathing air through accessory air-breathing organs or via gill system (Crampton, 1998; Moraes *et al*., 2002). Furthermore, fish are subjected to adverse situations such as large temperature fluctuations, food scarcity, and a broad spectrum of pathological agents (Bonga, 1997; Galindo *et al*., 2017).

Kidney anatomy of *G. inaequilabiatus* is arranged according to many other Teleostei fish (Takashima, Hibiya, 1995; Holz, Raidal, 2006). The head and exocrine portions are interconnected, with double branches that remain cranioventrally attached at the vertebral column. Dark brown was the predominant color due to their abundant vascular system and MMCs-rich parenchyma. Also, even though a wide variation is commonly reported, the RSI was similar to other fish species (Stoskopf, 2010). White cystic lesions focally distributed and with a firm consistency characterized the gross lesions. These lesions are common in free range fish populations and are associated with a wide variety of causes (Ferguson, 2006; Pavanelli *et al*., 2008; Bruno *et al*., 2013).

Tab. 2. Descriptive statistic values for structural volumetric densities (%) and Pearson. [#] considering 10 fields per specimen; SD, standard deviation; MMCs, melonomacrophages centers; [a] include arterioles, venule, and capillaries; [b] glomerulus with Bowman's capsule; [*] $p < 0.05$; [**] $p < 0.01$.

Head kidney[#]	Percentis				r
	Mean	SD	25th	75th	
Lymphohematopoietic tissue	65.7	9.31	60.7	72.0	0.20[*]
Sinusoidal lumen	17.1	3.32	12.7	20.7	ns
MMCs	12.1	7.41	6.0	16.0	-0.22[*]
Blood vessels[a]	3.3	5.84	0.0	6.7	ns
Granulomatous lesions	1.69	5.43	0.0	2.0	ns
Exocrine kidney[#]					
Lymphohematopoietic tissue	30.8	6.72	26.0	36.0	0.31[**]
Proximal tubule	28.5	8.12	22.7	34.0	0,45[*]
MMCs	14.24	6.91	9.3	18.9	-0.31[**]
Distal tubule	12.13	3.91	9.3	14.7	0.49[**]
Blood vessels[a]	10.50	9.13	4.7	13.3	0.21[**]
Granulomatous lesions	3.22	2.74	1.3	4.0	0.29[**]
Renal corpuscle[b]	0.49	0.41	0.00	0.70	ns

Tab. 3. Descriptive statistics values for histometric measures and Pearson's. [#] considering at least 5 structures in 10 images per specimen; Rgrc = glomerular area/renal corpuscle area ratio; RBrc = Bowman´s space area/renal corpuscle area ratio; ns, not significant; [*] $p < 0.05$; [**] $p < 0.01$.

	Percentis				r
	Mean	SD	25th	75th	
Renal corpuscle diameter (µm)	50.1	7.7	46.0	56.0	ns
Renal corpuscle area (µm²)	2,169.0	634.7	1,717.0	2,556.0	ns
Glomerular area (µm²)	1,831.7	586.7	1,400.0	2,186.0	ns
Bowman's space area (µm²)	337.1	161.6	212.0	416.0	ns
Rgrc (%)	83.9	7.7	79.0	89.4	ns
RBrc (%)	16.1	7.4	10.6	20.8	ns
Proximal tubular diameter (µm)	40.5	7.68	36.6	46.5	-0.38[**]
Proximal tubular thickness (µm)	15.6	2.30	13.7	18.0	-0.49[**]
Distal tubular diameter (µm)	44.4	17.9	29.5	55.7	ns
Distal tubular thickness (µm)	15.2	4.84	11.0	18.9	-0.23[**]

To date, there are no anatomical, histological or histopathological descriptions of the kidney in *G. inaequilabiatus*, which prevent a comparative analysis within the Gymnotiformes Genus. However, the values found of the relative volumetric density from the proximal tubules are similar to the sum of the proximal tubules I and II values reported in the *Salmo trutta* (Resende *et al*., 2010), in accordance to the low percentage of renal corpuscles. Both tubular segments were not estimated separately once the distinct morphological features are more clearly recognized by transmission microscopy (Takashima, Hibiya, 1995; Elger *et al*., 2000). Further restrictive comparisons, including other renal structures, are still speculative due to the limited numbers of stereological studies, although the overall tissue composition is analogous between kidneys of different fish species.

Given the wide variety on the morphological and anatomical kidney trends, the RSI was a useful measure since it correlated with several macroscopic and microscopic attributes. This index reflects the proportional sizes of organs relative to the body mass. Many environmental factors influence their variation and indicate the general status of the health of an individual organism (Strepparava *et al*., 2018). Although we have found a positive linear correlation with relative condition factor, the correlation with the number of gross lesions was high (r = 0.48, Tab. 1). Furthermore, the linear correlation with the volumetric density of MMCs was negative in both head (r = - 0.22) and exocrine portions (r = - 0.31, Tab. 2). The coefficient measured between gross lesions and RSI suggests that adult or aged specimens with higher indices would tend to sustain more injuries through the organ. The negative correlations with MMCs may be due to these structures remaining aggregated around the granulomatous lesions and moderately dispersed in the renal parenchyma, a feature previously reported to hepatic nematode-cysts granulomas (Galindo *et al*., 2017). In the present study, MMCs account for a substantial fraction of the volumetric density in both the head and exocrine kidney mostly composed of melanin (Agius, Roberts, 2003; Kumar *et al*., 2016). Hemosiderin and lipofuscin were promptly identified, although they have not been quantified. In addition to the immune function, MMCs are involved in the endogenous phagocytosis material of exhausted cells, particularly erythrocytes. Thus, these structures in both kidneys may be implicated in a stable iron-recycling function and antimicrobial response (Steinel, Bolnick, 2017; Grayfer *et al*., 2018). The volumetric density of MMCs is consistent with those reported in *Salvelinus fontinalis* and *Oncorhynchus mykiss*, even though the measurement techniques of their content have been different (Schwindt *et al*., 2006). In contrast with this study, granulomatous lesions do not appear to be an occasional finding once were frequently observed in all samples in *G. inaequilabiatus*.

The volumetric density of lymphohematopoietic tissue was measured independently between the head and exocrine portions, once both portions were morphologically delimited and microscopically distinguishable. It constituted the highest relative volumetric density percentage of structures evaluated in both portions. However, in the exocrine kidney except for the renal corpuscle, all structures observed were associated with RSI, suggesting that renal volume dynamics depend on subtle pathophysiological adjustments. The nephrogenesis in adult fish seems to be a continuous regenerative process related to fish body size and nephron number (Reimschuessel, 2001; Davidson, 2011). The proximal and distal tubule segments showed highest correlations, and both are functionally active for osmoregulation, urea, creatinine, amino acids and glucose homeostasis (Larsen, Perkins Jr., 2005; Dantzler, 2016). Also, proximal tubules presented typical and irregular

eosinophilic hyaline granules, probably in accordance with reabsorption of excess amounts of proteinaceous substances depurated from the glomerulus. This process has been observed under both pathological and healthy fish (Takashima, Hibiya, 1995; Wolf *et al*., 2015).

The head and exocrine kidney presented an appreciable vascular network. The expressive volumetric density of sinusoidal lumen suggests a similar function to that performed by the spleen, where foreign bodies, such as bacterial, fungal or parasitic fragments are trapped within a fine reticular meshwork (Fergusson, 2006; Roberts, Ellis, 2012). While in the head portion the sinusoidal lumen was prominently configuring meaningful flow irrigation among the lymphohematopoietic cell niches, the blood vessels were prominent in the exocrine portion. However, only blood vessels from the exocrine portion correlated to RSI. Indeed, in most teleost fish, the glomerular blood supply is arterial while the renal tubules have a second supply of blood; the first emerge from the efferent glomerular arterioles, and the second from the venous renal-portal system (Hentschel *et al*., 2000; Holz *et al*., 2006). Thus, considering the higher density of proximal and distal tubules distributed throughout the tissue, the venous vasculature may be regarded as a notable feature in this species. The interactive, functional, and volumetric density aspects of tubular and parenchymal vasculature retained an expressive account on the RSI estimative.

Histometric measures contribute to the description of the tissue shape and functionality, which varies according to the species characteristic and might express different levels of healthiness (Reid, 1980; Nyengaard, 1999). Proximal and distal tubular measures are related to plasticity and remodeling of epithelial cells in response to reabsorption and excretory function in teleosts fish adapted to freshwater (Oğuz, 2015; Dantzler, 2016). The proximal tubular diameter and thickness, as well as distal tubular thickness, were negatively correlated with RSI. These measures implicate in size-attributes and may modulate this index since both segments represented the highest percentage of renal structures. Our results suggest that lower and narrower tubules would be concentrated in adults and heavier specimens with more significant renosomatic indices.

We described for the first time the morphological baseline in light microscopy of *G. inaequilabiatus*. The RSI is associated with various functional structures, and their variation accounts significantly for the volumetric density of lymphohematopoietic tissue, as well as of the proximal and distal tubular segments. The prevalence of granulomatous lesions in both kidney portions indicate to us that these act as target-organs for arresting foreign bodies, composing a critical immune response in this species. This particularity, along with MMCs relative density and pigmentary characteristics could address us news essays in order to elucidate the renosomatic index relation to environmental factors.

References

Agius C, Roberts RJ. Melano-macrophage centres and their role in fish pathology. J Fish Dis. 2003; 26(9):499–509. https://doi.org/10.1046/j.1365-2761.2003.00485.x

Albert JS, Crampton WGR, Thorsen DH, Lovejoy NR. Phylogenetic systematics and historical biogeography of the Neotropical electric fish *Gymnotus* (Teleostei: Gymnotidae). Syst Biodivers. 2005; 2(4):375–417. https://doi.org/10.1017/S1477200004001574

Bonga SEW. The stress response in fish. Physiol Rev. 1997; 77(3):591–625. https://doi.org/10.1152/physrev.1997.77.3.591

Bruno DW, Noguera PA, Poppe TT. A colour atlas of salmonid diseases. 2nd ed, UK: Springer Science BMBV; 2013.

Carson FL, Hlakik C. Histotechnology. A self-instructional text. 3rd ed, Hong Kong: ASCP Press; 2009.

Crampton WGR. Effects of anoxia on the distribution, respiratory strategies and electric diversity of gymnotiform fishes. J Fish Biol. 1998; 53:307–30. https://doi.org/10.1111/j.1095-8649.1998.tb01034.x

Cuesta A, Meseguer J, Esteban MA. Immune and osmoregulatory system interaction. In: Baldisserotto B, Mancera JM, Kapoor BG, editors. Fish osmoregulation. Enfield: Science Publishers; 2007. p.1–34.

Dantzler WH. Renal Morphology. In: Comparative physiology of the Vertebrate kidney. New York: The American Physiological Society, Springer, 2016. p.7–36.

Davidson AJ. Uncharted waters: nephrogenesis and renal regeneration in fish and mammals. Pediatr Nephrol. 2011; 26(9):1435–43. https://doi.org/10.1007/s00467-011-1795-z

Dethloff GM, Schmitt CJ. Conditions factors and organosomatic indices. In: Schmitt CJ, Dethloff GM, editors. Biomonitoring of environmental status and trends (BEST) program: selected methods for monitoring chemical contaminants and their effects in aquatic ecosystems. U.S. Geological Survey, Biological Resources Division, Columbia, (MO): Information and Technology Report USGS/BRD-2000—0005, 2000. p.13–25.

Elger M, Hentschel H, Dawson M, Renfro JL. Urinary tract. In: Ostrander GK, editor. The handbook of experimental animals. The laboratory fish. San Diego: Academic Press; 2000. p.385–413.

Ferguson HW. Systemic pathology of fish: a text atlas of normal tissues in teleosts and their responses in disease. London: Scotian Press; 2006.

Franco-Belussi L, Santos LRS, Zieri R, Vicentini CA, Taboga SR, Oliveira C. Liver anatomy, histochemistry, and ultrastructure of *Eupemphix nattereri* (Anura: Leiuperidae) during the breeding season. Zool Sci. 2012; 29(12):844–48. https://doi.org/10.2108/zsj.29.844

Freere RH, Weibel ER. Stereologic techniques in microscopy. J Roy Microscopic Soc. 1967; 87(1):25–34. https://doi.org/10.1111/j.1365-2818.1967.tb04489.x

Fricke R, Eschmeyer WN, Fong JD. Eschmeyer's catalog of fishes: species by Family/Subfamily. [Internet]. San Francisco: California Academy of Science; 2019. Available from: http://researcharchive.calacademy.org/research/ichthyology/catalog/SpeciesByFamily.asp

Galindo GM, Rodrigues RA, Marcondes SF, Soares P, Tavares LER, Fernandes CE. Morphological and morphometric features of nematode-cysts in *Gymnotus inaequilabiatus* liver in the Brazilian Pantanal. Rev Bras Parasitol Vet. 2017; 26(3):285–91. http://dx.doi.org/10.1590/s1984-29612017044

Grayfer L, Kerimoglu B, Yaparla A, Hodgkinson JW, Xie J, Belosevic M. Mechanisms of fish macrophages antimicrobial immunity. Front Immunol. 2018; 9(1105):1–22. https://doi.org/10.3389/fimmu.2018.01105

Hamilton PW, Bankhead P, Wang Y, Hutchinson R, Kieran D, McArt DG, James J, Salto-Tellez M. Digital pathology and image analysis in tissue biomarker research. Methods. 2014; 70(1):59–73. https://doi.org/10.1016/j.ymeth.2014.06.015

Harper C, Wolf JC. Morphological effects of the stress response in fish. ILAR J. 2009; 50(4):387–96. https://doi.org/10.1093/ilar.50.4.387

Hassan MM, Defaveri J, Kuure S, Dash SN, Lehtonen S, Merila J, Mccaims RJS. Sticklebacks adapted to divergent osmotic environments show differences in plasticity for kidney morphology and candidate gene expression. J Exp Biol. 2017; 220(12):2175–86. https://doi.org/10.1242/jeb.146027

Hentschel H, Elger M, Dawson M, Renfro JF. Urinary Tract. In: Ostrander JK, editor. The handbook of experimental animals. The laboratory fish. San Diego: Academic Press; 2000. p.175–81.

Holz PH, Raidal SR. Comparative renal anatomy of exotic species. Vet Clin North Am Exot Anim Pract. 2006; 9(1):1–11. https://doi.org/10.1016/j.cvex.2005.09.001

Jordanova M, Rocha MJ, Rebok K, Rocha E. Variations in the volumes of parenchyma and stroma of the liver and in the cytology of hepatocytes are associated with gonadal stages in female Ohrid trout (*Salmo letnica*). Ichthyol Res. 2013; 60(1):26–35. https://doi.org/10.1007/s10228-012-0302-2

Kumar R, Joy KP, Singh SM. Morpho-histology of head kidney of female catfish *Heteropneustes fossils*: seasonal variations in melano-macrophage centers, melanin contents and effects of lipopolysaccharide and dexamethasone on melanin. Fish Physiol Biochem. 2016; 42(5):1287–306. https://doi.org/10.1007/s10695-016-0218-2

Larsen BK, Perkins Jr. EJ. Target organ toxicity in the kidney. In: Schlenk D, Benson WH, editors. Target organ toxicity in marine and freshwater teleosts: organs. London and NewYork: Taylor & Francis; 2005. p.102–64.

Le Cren ED. The length, weight relationship and seasonal cycle in gonad weight and condition factor in the perch (*Perca fluviatilis*). J Anim Ecol. 1951; 20(2):201–19. www.jstor.org/stable/1540

Menke AL, Spitsbergen JM, Wolterbeek APM, Woutersen RA. Normal anatomy and histology of the adult zebrafish. Toxicol Pathol. 2011; 39(5):759–75. https://doi.org/10.1177/0192623311409597

Moraes G, Avilez IM, Altran AE, Barbosa CC. Biochemical and hematological responses of the banded knife fish *Gymnotus carapo* (Linnaeus, 1758) exposed to environmental hypoxia. Braz J Biol. 2002; 62(4A):633–40. http://dx.doi.org/10.1590/S1519-69842002000400011

Nyengaard JR. Stereologic methods and their application in kidney research. J Am Soc Nephrol. 1999; 10(5):1100–23. https://jasn.asnjournals.org/content/10/5/1100

Oberholzer M, Östreicher M, Christen H, Brühlmann M. Methods in quantitative image analysis. Histochem Cell Biol. 1996; 105(5):333–55. https://doi.org/10.1007/BF01463655

Oğuz AR. A histological study of the kidney strucutures of Van fish (*Alburnus tarichi*) acclimated to hight alcaline water and freswater. Mar Freshw Behav Physiol. 2015; 48(2):133–44. https://doi.org/10.1080/10236244.2015.1004838

Pavanelli GC, Eiras JC, Takemoto RM. Doenças de peixes. Profilaxia, diagnóstico e tratamento. 3rd ed, Maringá: EDUEM; 2008.

Pelster B, Wood CM, Jung E, Val AL. Air-breathing behavior, oxygen concentrations, and ROS defense in the swimbladders of two erythrinid fish, the facultative air-breathing jeju, and the non-air-breathing traira during normoxia, hypoxia and hyperoxia. J Comp Physiol B. 2018; 188(3):437–49. https://doi.org/10.1007/s00360-017-1142-1

Reid IM. Morphometric methods in veterinary pathology: a review. Vet Pathol. 1980; 17(5):522–43. https://doi.org/10.1177/030098588001700502

Reimschuessel R. A fish model of renal regeneration and development. ILAR J. 2001; 42(4):285–91. https://doi.org/10.1093/ilar.42.4.285

Resende AD, Lobo-Da-Cunha AL, Malhão F, Franquinho F, Monteiro RAF, Rocha E. Histological and stereological characterization of brown trout (*Salmo trutta* f. fario) trunk kidney. Microsc Microanal. 2010; 16(6):677–87. https://doi.org/10.1017/S1431927610093918

Resende EK, Pereira RAC, Sório VF, Galvão EM. Biologia da tuvira, *Gymnotus* cf. *carapo* (Pisces, Gymnotidae) no baixo rio Negro, Pantanal, Mato Grosso do Sul, Brasil. Corumbá: Embrapa Pantanal; 2006.

Roberts RJ, Ellis AE. The anatomy and physiology of teleosts. In: Roberts JR, editor. Fish Pathology. UK: Wiley-Blackwell Publishing; 2012. p.17–61.

Rocha E, Monteiro RAF, Pereira CA. Liver of the brown trout, *Salmo trutta* (Teleostei, Salmonidae): a stereological study at light and electron microscopic levels. Anat Rec 1997; 247(3):317–28. https://doi.org/10.1002/(SICI)1097-0185(199703)247:3<317::AID-AR3>3.0.CO;2-R

Scacchetti PC, Pansonato-Alves JC, Utsunomia R, Oliveira C, Foresti F. Karyotypic diversity in four species of the genus *Gymnotus* Linnaeus, 1758 (Teleostei, Gymnotiformes, Gymnotidae): physical mapping of ribosomal genes and telomeric sequences. Comp Cytogenet. 2011; 5(3):223–35. https://doi.org/10.3897/CompCytogen.v5i3.1375

Schwindt AR, Truelove N, Schreck CB, Fournie JW, Landers DH, Kent ML. Quantitative evaluation of macrophage aggregates in brook trout *Salvelinus fontinalis* and rainbow trout *Oncorhynchus mykiss*. Dis Aquat Organ. 2006; 68(2):101–13. https://doi.org/doi:10.3354/dao068101

Shibutani M, Uneyama C, Miyazaki K, Toyoda K, Hirose M. Methacarn fixation: a novel tool for analysis of gene expressions in paraffin-embedded tissue specimens. Laboratory Investigation. 2000; 80(2):199–208. https://www.nature.com/articles/3780023

Schlenk D, Calander M, Gallagher EP, Gorge S, James M, Kulman SW, Van Den Hurk P, Willet K. Biotransformation in fish. In: Di Giulio RT, Hinton DE, editors. The toxicology of fishes. USA: CRC Press; 2008. p.154–234.

Steinel NC, Bolnick DI. Melanomacrophages centers as a histological indicator of immune functions in fish and other poikilotherms. Frontiers Immunol. 2017; 8:1–8. https://doi.org/10.3389/fimmu.2017.00827

Stoskopf M. Fish Medicine. 2nd ed, W.B. Saunders Company, 2010.

Strepparava N, Segner H, Ros A, Hartikainen H, Schmidt-Posthaus H, Wahli T.

Temperature-related parasite infection dynamics: the case of proliferative kidney disease of brown trout. Parasitol. 2018; 145(3):281–29. https://doi.org/10.1017/S0031182017001482

Takashima F, Hibiya T. An atlas of fish histology: normal and pathological features. 2nd ed, Tokyo: Kondansha; 1995.

Willink PW, Chernoff B, Alonso LE, Montambault JR, Lourival R. RAP bulletin of biological assessment. Washington: Library of Congress Card; 2000.

Wolf JC, Baumgartner WA, Blazer VS. Nonlesions, misdiagnosis, missed diagnoses and other interpretative challenges in fish histopathology studies: a guide for investigators, authors, reviewers, and readers. Toxicol Pathol. 2015; 43(3):297–325. https://doi.org/10.1177/0192623314540229

Zapata AG, Chibá A, Varas A. Cells and tissues of the immune system of fish. In: Iwama G, Nakanishi T. The fish immune system. Organism, pathogen, and environment. EUA: Academic Press; 1996. p.1–53.